

Preparation and characterization of MgO nanoparticles/ferroelectric liquid crystal composites for faster display devices with improved contrast†

Cite this: *J. Mater. Chem. C*, 2014, 2, 1844

Achu Chandran,^a Jai Prakash,^{*b} Kush Kumar Naik,^a Avanish Kumar Srivastava,^a Roman Dąbrowski,^c Michał Czerwiński^c and A. M. Biradar^a

In this article, we present the formulation and characterization of a ferroelectric liquid crystal (FLC) mixture W301 composed of pyrimidine compounds. We observed that upon doping magnesium oxide nanoparticles (MgO NPs) into the host FLC, the MgO NPs/FLC composite showed significantly faster response and improved optical tilt angle. The decreased response time in the MgO NPs/FLC composite has been attributed to the decrease in rotational viscosity and increase in surface anchoring energy. The decrease in rotational viscosity of the composite is due to the torque experienced by both MgO NPs and FLC in the presence of an electric field and perturbations of order parameters of FLC. Due to the enhanced surface interaction of MgO NPs having surface defects with mesogens, strong surface anchoring is experienced on the FLC molecules that not only increased the speed of the response but also improved the optical tilt angle of the MgO NPs/FLC composites, which ultimately resulted in improved contrast. A systematic approach has been followed to elucidate the idea of designing faster display devices with improved contrast based on MgO NPs/FLC composites.

Received 12th October 2013
Accepted 27th November 2013

DOI: 10.1039/c3tc32017k

www.rsc.org/MaterialsC

Introduction

Liquid crystals (LCs) constitute a fascinating state of condensed matter which is widely utilized in electro-optical applications due to their attractive physical anisotropic properties. High resolution, light weight, compactness and low power consumption with good enough image quality make LC display devices more popular than other counterparts. Still, these devices need improvement as they have slow responses and limited viewing angles as compared to electroluminescent displays. Faster operating LC materials are needed for colour sequential and true 3D LCDs.^{1,2} Ferroelectric LCs (FLCs), special members of the LC family, have attracted considerable attention from fundamental and applied aspects because of their faster response, low threshold voltage, memory effect *etc.*³⁻⁶ Even FLCs need improvement in electro-optical characteristics for use in next generation advanced display devices with wide

viewing angles, fast electro-optic responses and good optical contrast. In the case of FLCs, getting good alignment of mesogens on large scale flat panels is also a difficult task. On the other hand, attempts were started by researchers to enhance the electro-optical properties of LCs by the incorporation of nanometric size particles to the LC host matrix to form nanoparticles (NPs)/LC composites having novel dynamic properties different from the original LC medium due to perturbation of the self-assembly properties of the LCs. The nano-materials reported as a dispersed phase in LCDs involve fullerene, carbon nanotubes, diamond powder, noble metal NPs, and semiconductor NPs *etc.*⁷⁻¹¹ When these nano-materials are used as a dopant for LCDs then the latter are expected to show improved contrast, ion capture, high voltage holding ratio, frequency modulation response and decreased driving voltage. Most of the work in this area is based on nematic LCs; especially for display applications. The observed enhancement of electro-optical properties of these composites is attributed to the changes in the order parameters and the increase of steric interaction between LC molecules and NPs, which produces a significant alteration of the properties of the LCs such as dielectric anisotropy, birefringence, elastic constants, viscosity *etc.* Also, the preparation of nanocomposites based on LC mixtures and inorganic NPs is an effective way to tune the electronic and optical properties of the NPs/LC system with the functional and structural flexibilities of the host LC materials.

^aCSIR-National Physical Laboratory, Dr. K. S. Krishnan Road, New Delhi – 110012, India

^bCentre for Physical and Mathematical Sciences, School of Basic and Applied Sciences, Central University of Punjab, City Campus, Mansa Road, Bathinda – 151001, Punjab, India. E-mail: jpsphysics@gmail.com

^cInstitute of Chemistry, Military University of Technology, ul. Kaliskiego 2, 00-908 Warsaw, Poland

† Electronic supplementary information (ESI) available. See DOI: 10.1039/c3tc32017k

As a dopant for LCs, metal oxide NPs are interesting materials with fascinating properties and have attracted immense interest in the scientific community because of their unique physical and chemical properties resulting from their limited size and a high density of corner or edge surface sites.^{12–15} Metal oxides can adopt a vast number of structural geometries with an electronic structure that can exhibit metallic, semiconducting or insulating character. They are used in various technological applications, such as microelectronic circuits, sensors, piezoelectric devices, fuel cells, coatings for the passivation of surfaces against corrosion, and catalysts. Among all metal oxide NPs, magnesium oxide nanoparticles (MgO NPs) have unique physical and chemical properties due to high surface areas and structural defects compared with bulk MgO. Nanosized MgO is widely used as a scrubber for air pollutant gases in the chemical industry and as a catalyst support.¹⁶ They have active chemical sites with high binding energies, and are attractive candidates for application as sensors and heterogeneous catalysts.¹⁷ More interestingly, the presence of oxygen vacancies in MgO NPs has a tremendous influence on their electronic and chemical properties.¹⁸

Upon dispersing poly(cyclodextrin)-capped silica (PCy-SiO₂) NPs into nematic LCs, Shiraiishi *et al.* were able to construct a novel twisted nematic LC with a faster response time.¹⁹ Gardiner *et al.* reported a faster switching electro-optical device with high contrast based on the in-plane switching of a very short pitch polymer stabilized chiral nematic LC.²⁰ Later, some authors observed the decreasing of the response time of FLCs upon doping BaTiO₃ NPs and poly(3,4-ethylene-dioxythiophene) nanotubes into the host FLCs.^{21,22} Recently, our group has observed a faster response of deformed helix ferroelectric liquid crystal (DHFLC) material and FLC material upon doping multi-walled carbon nanotubes (MWCNTs) and copper oxide decorated MWCNTs into the host material.^{23,24} Metal oxide NPs doping in FLCs for enhancement of electro-optical properties of the host materials is rarely reported. Some recent studies on doping of MgO NPs on nematic LC composites have been reported. Haraguchi *et al.* reported the reduction of the threshold voltage of a twisted nematic LC cell which was caused by doping with NPs of MgO and SiO₂. The authors discussed the mechanism of these phenomena and attributed the reduction of the threshold voltage to the reduction of the order parameters by doping NPs.²⁵ Sano *et al.* demonstrated that LC displays based on twisted nematic, tunable birefringence, vertically aligned nematic, and bent nematic-modes exhibited reduction in the operating voltage and response times upon doping with MgO NPs.²⁶ To the best of our knowledge there are no reports on the improvement of electro-optical properties of FLCs by doping with MgO NPs.

The present study focuses on the formulation and characterization of a new FLC material, namely W301 and the effect of doping MgO NPs on the enhancement of the electro-optical properties such as faster response time and improved tilt angle of the host FLC. The decrease of the response time in the MgO NPs/FLC composite has been attributed to the decrease in rotational viscosity and increase in surface anchoring energy. Also, the role of the anchoring strength of mesogens and MgO NPs on the better contrast of the composite resulting from the increased optical tilt is discussed. This article systematically

presents the feasibility of fabricating MgO NPs/FLC composites having faster response times with improved contrast for future display applications and other electro-optical applications, such as beam steering or polarization shutters.

Experimental

Formulation of new FLC mixture, W301

The main components of the FLC mixture W301 are pyrimidine compounds and chiral terphenyl dopant.^{27,28} The composition of mixture W301 is shown in Table 1.

Synthesis of MgO NPs

Nanosized particles of MgO were synthesized *via* a hydrothermal method from magnesium nitrate (MgNO₃·6H₂O), sodium hydroxide (NaOH) and de-ionized water (H₂O) as precursors in appropriate amounts. Here, we added 5.1282 g of MgNO₃·6H₂O into 100 ml of de-ionized water in a beaker containing a magnetic stirrer and subsequently, 2 g of NaOH, which was dissolved in 100 ml of de-ionized water, was added dropwise to the MgNO₃·6H₂O solution. The pH value of the resultant solution was 12.5 and it appeared a white colour. The precipitate was filtered and washed with methanol three to four times to remove ionic impurities. The filtered dry powder was annealed at 500 °C for about two hours to obtain MgO NPs.

Liquid crystal sample cell fabrication

The LC sample cells were fabricated using highly conducting (30 ohm □⁻¹) and optically transparent sputtered indium tin oxide (ITO) glass substrates. The desired electrode patterns having areas of 0.45 × 0.45 cm² were obtained by using a photolithographic (using positive photo resist) technique. The homogeneous alignment of LC sample cells was achieved by using a conventional rubbed polyimide technique. The thickness of the cell was maintained by using 6 μm thick Mylar spacers. Detailed experimental processes for the fabrication of LC sample cell are listed in the ESI.†

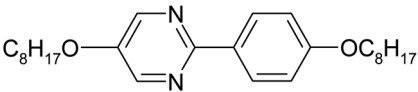
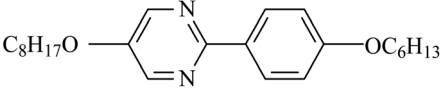
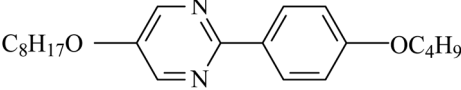
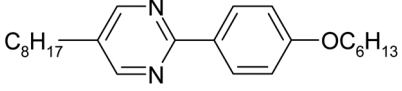
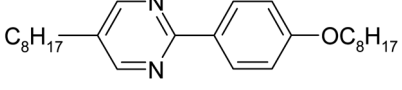
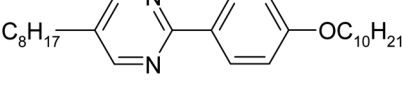
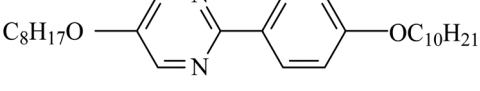
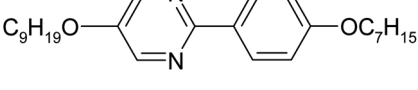
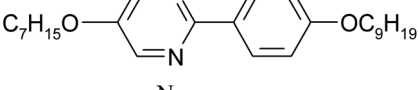
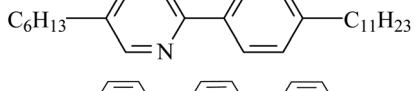
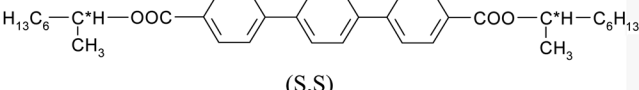
Preparation of MgO NPs/FLC composite

The MgO NPs/FLC composite was prepared by adding various concentrations (wt%) of nanopowder of MgO NPs to the FLC material. The mixture was then ultrasonicated for about 40 min in the isotropic phase of the FLC material to ensure the homogeneous dispersion of MgO NPs in the FLC host material. The pure and MgO NPs (of different concentration and sizes) doped W301 materials were then introduced into the LC sample cells by means of capillary action at a temperature just above the isotropic transition temperature.

Apparatus and measurements

The dielectric permittivity and dielectric loss factors of the pure and doped cells were measured using an impedance analyzer (Wayne Kerr 6540 A, U. K.) in a frequency window of 20 Hz–1 MHz with a measuring voltage of 0.5 V_{pp}. A temperature controller (JULABO F-25 HE) was used for controlling the

Table 1 Composition of the mixture W301

| Component no. | Structure of compounds in W301 | Concentration [wt%] |
|---------------|--|---------------------|
| 1 |  | 15.18 |
| 2 |  | 11.43 |
| 3 |  | 17.83 |
| 4 |  | 15.93 |
| 5 |  | 12.35 |
| 6 |  | 4.40 |
| 7 |  | 2.44 |
| 8 |  | 2.07 |
| 9 |  | 4.68 |
| 10 |  | 8.69 |
| 11 |  | 5.00 |

temperature with a temperature stability of ± 0.01 °C. The sample holder containing the sample cells was kept thermally isolated from the external sources for carrying out the temperature dependent studies. The optical tilt angle and micrographs of the sample cells were recorded with the help of a polarizing optical microscope (Ax-40, Carl Zeiss, Germany) fitted with a charge coupled device (CCD) camera. The material parameters of the FLC sample cells such as rotational viscosity and spontaneous polarization were determined by using an automatic liquid crystal tester (ALCT, Instec, USA). High resolution transmission electron microscopy (HRTEM) experiments were performed by using an HRTEM model Tecnai G2 F30 STWIN operated at the electron accelerating voltage of 300 kV using an electron source as the field emission gun. The phase transition

temperatures and enthalpies were measured by the Differential Scanning Calorimetric (DSC) method (Setaram 141). The photoluminescence (PL) spectrum of the MgO NPs was investigated by using a PL instrument, a Perkin-Elmer LS-55 luminescence spectrometer (Xe source). The intensities of the dark and bright states of the pure and doped samples were compared using a high resolution spectrometer, Ocean Optics Inc., HR 4000.

Results and discussions

Characterization of MgO NPs

Detailed electron microscopy observation revealed several interesting features of the MgO NPs in real and reciprocal space. Fig. 1(a) shows an ultra-fine highly dense collection of NPs of

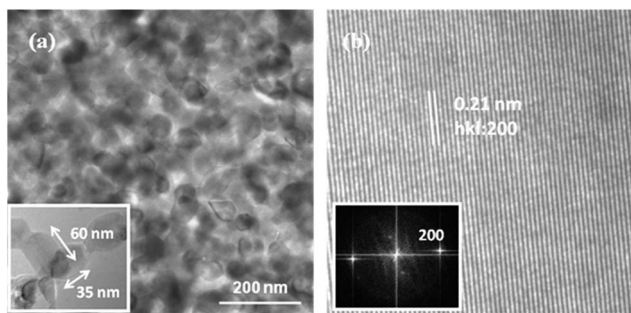


Fig. 1 HRTEM images showing (a) distribution of high yield of nano-particles and (b) an atomic scale image with the presence of (200) planes of a cubic crystal. Insets: (a) individual nano-particles with clear facets and edges, and (b) corresponding FFT of atomic scale image.

rounded-polyhedral shape throughout the material. Several such regions were recorded while carrying out electron microscopy experiments.

On an average the size of these NPs ranged between 30 and 60 nm with an average size of about 50 nm. At high magnifications, it has been noticed that the individual particles are faceted with sharp edges and notches showing a preferred growth along certain crystallographic planes during the synthesis. A few NPs with faceted morphologies are displayed in the inset in Fig. 1(a). Two such NPs with facets having lengths of their edges of about 60 and 35 nm are marked on the micrograph (inset in Fig. 1(a)). An atomic scale image (Fig. 1(b)) of an individual NP clearly exhibits that the particle is constituted of a stacking sequence of $hkl: 200$ planes with an inter-planar spacing of 0.21 nm of a cubic crystal structure of MgO (ref.: JCPDS file no. 870652, lattice parameter: $a = 0.4211$ nm). The stacking of (200) planes is atomically clean without any imperfections at the lattice scale within the particle. A corresponding fast Fourier transform image (FFT), as in the inset of Fig. 1(b)) of the lattice scale image in reciprocal space further authenticates the presence of (200) planes constituting the NP.

Characterization of the prepared FLC, W301

The prepared FLC material, W301, has been characterized by using various experimental techniques, such as dielectric relaxation spectroscopy, polarization optical microscopy (POM) and other electro-optical studies. The dielectric permittivity and dielectric loss factor of W301 as a function of frequency at room temperature are shown in Fig. 2.

The dispersion curve clearly shows that the newly prepared FLC material possesses a dielectric permittivity of the order of 45 at 20 Hz. Fig. 2 also shows the absorption curve (dielectric loss factor, $\tan \delta$), where a beautiful relaxation peak is clearly seen which occurs at a frequency of ~ 0.7 kHz in the absorption spectrum of W301. This relaxation peak is connected with the phase fluctuations in the azimuthal orientation of the director, called the Goldstone mode (GM).^{29–31} The material parameters such as spontaneous polarisation, rotational viscosity, response

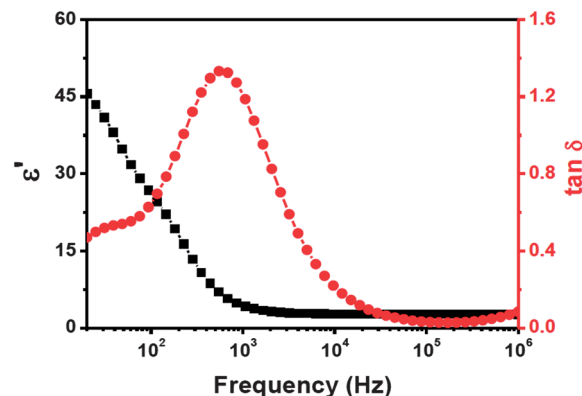


Fig. 2 Behaviour of dielectric permittivity (ϵ') and dielectric loss factor ($\tan \delta$) as a function of log of the frequency at room temperature of the FLC material W301 with cell thickness of 6 μm in planar alignment configuration.

time and tilt angle of the newly synthesized FLC material, W301, with applied voltage at room temperature are shown in Fig. 3.

The spontaneous polarization is calculated by using the triangular wave method in which a triangular wave of desired amplitude and frequency was applied across the sample cell and the response of the output current was recorded using an oscilloscope. The calculated area under the output current curve gives the spontaneous polarization by using the formula $2aP_s = \text{area under the curve}$; where a is the active area of the sample cell and P_s is the spontaneous polarization. The response time is calculated by the square wave method, in which the distance between the edges of the square and the polarization hump on the time axis gives the response time. For an estimation of the rotational viscosity, the relationship below is used:

$$\gamma = \tau P_s E \quad (1)$$

where γ is the rotational viscosity, P_s is the spontaneous polarization, and E is the applied field. As seen from Fig. 3(a), the saturation value of spontaneous polarization is around 11 nC cm^{-2} and the magnitude of rotational viscosity is around 120 mPa s at room temperature (25 $^\circ\text{C}$). Fig. 3(b) shows the response time, which is of the order of sub-milliseconds and the saturation value of tilt angle, which is observed at around 17 $^\circ$ at 25 $^\circ\text{C}$.

The different phase assignments and corresponding transition temperatures were determined at atmospheric pressure by DSC. One can see various peaks corresponding to the phase transitions of the mixture W301 from Fig. 4 which shows the DSC trace obtained for the cooling cycle.

From Fig. 4, three peaks are easily observed, 1, 2, and 4, which are connected with phase transitions from the isotropic to nematic phase (Iso-N*), nematic to smectic A* phase (N*-mA*) and smectic C* to crystalline phase (SmC*-Cr), respectively. Peaks 1 and 2 are narrowly separated, because the nematic phase of the material occurs over a very small range (~ 0.3 $^\circ\text{C}$). The phase transition SmA*-SmC* is nearly second-order and therefore it is visible as a very small peak (peak 3),

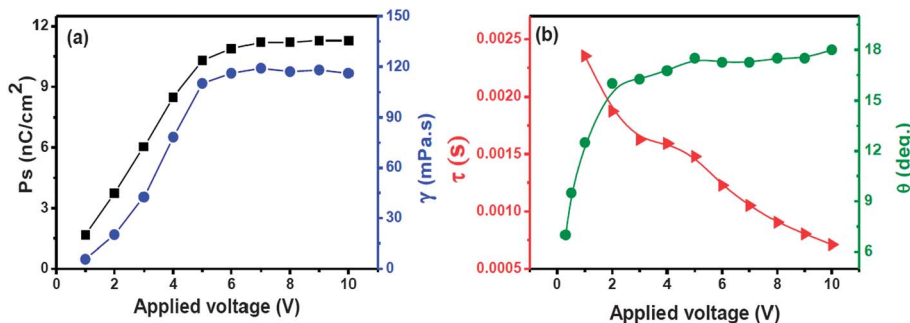


Fig. 3 Material parameters of the FLC material W301. Behavior of (a) spontaneous polarization (P_s) (black filled square symbol) and rotational viscosity (γ) (blue filled circular symbol), (b) response time (τ) (red filled triangle symbol), and optical tilt angle (θ) (green filled circular symbol) with applied voltage at room temperature.

which is enlarged and shown in the inset in Fig. 4. The heating trace is not presented because the transitions are broad.

Fig. 5 shows the variation of $\tan \delta$ with frequency at different temperatures ranging from 10 °C to 60 °C. This absorption curve gives a clear idea about the phase transition of the FLC material, W301, from the smectic C* phase to the smectic A* phase.

In Fig. 5, it is clearly visible that at 59 °C, the GM relaxation peak has disappeared and a new relaxation peak at a frequency of $\sim 10^4$ kHz has appeared. This relaxation peak has a lower loss value than that due to the GM and is called the Soft mode,^{30,32} which usually occurs near the smectic C*–smectic A* phase transition and is due to fluctuations in the amplitude of the tilt angle. The transition temperature of the material was further confirmed by textural observations by using POM. For this, the optical textures of the material under crossed polarisers were recorded at various temperatures indicating phase transitions of the material.

Fig. 6 shows the optical micrographs of the pure FLC material W301 filled cell of 100 μm thickness without any

surface treatment at temperatures of 30 °C, 59 °C, 70 °C, 80.5 °C, 80.7 °C and 80.8 °C. The dechiralisation lines, which are the characteristic property of the smectic C* phase and occur due to the helical nature of the director, are visible in Fig. 6(a). Also, the switching of mesogens took place at this temperature upon the application of the electric field. As the temperature of the sample was increased, the dechiralisation lines and switching properties started to disappear and at 59 °C, the switching had completely disappeared (Fig. 6(b)). This observation leads to the conclusion that the transition from smectic C*–smectic A* phase occurs at 59 °C in the FLC material W301. Fig. 6(c) shows the optical micrograph of the material at 70 °C, where the material is purely in the smectic A* phase. Upon further increasing the temperature, at 80.5 °C (Fig. 6(d)), a nematic type texture appeared for small range of temperatures and the intensity started to decrease further (Fig. 6(e)). At 80.8 °C, the sample appears completely dark which indicates the isotropic phase of the sample (Fig. 6(f)). From all the above-mentioned observations, *i.e.*, DSC, dielectric relaxation spectroscopy and textural studies, the phase

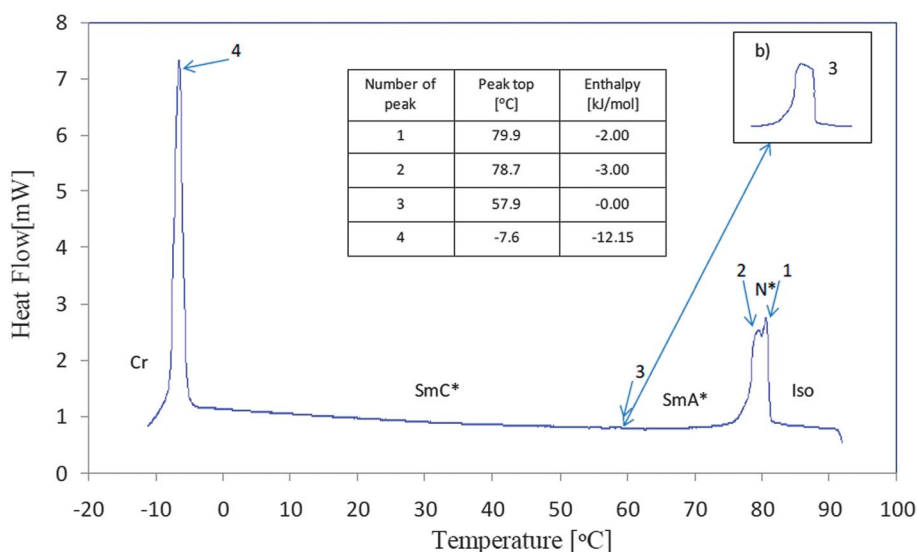


Fig. 4 DSC trace during cooling of the mixture W301.

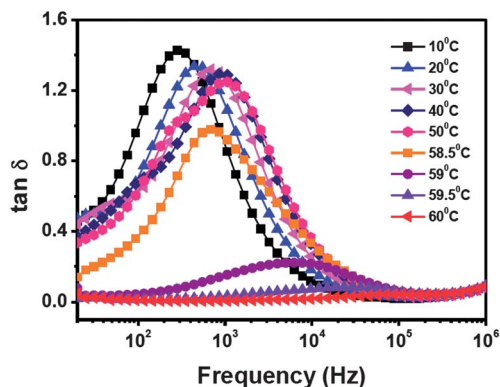
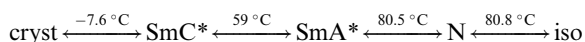


Fig. 5 Behaviour of the dielectric loss factor ($\tan \delta$) as a function of the log of the frequency of the FLC material W301 with a cell thickness of $6 \mu\text{m}$ in planar alignment configuration at different temperatures from 10 – 60°C .

sequence of the newly synthesized FLC material W301 can be given as follows:



where *cryst* is the crystalline phase, *SmC** is the chiral smectic C phase, *SmA** is the chiral smectic A phase, *N* is the nematic phase, and *iso* is the isotropic phase.

Faster electro-optic response of MgO NPs/FLC composites

The electro-optic response time at room temperature (25°C) for various concentrations of the MgO NPs doped FLC material W301 as a function of applied voltage and a comparison with pure W301 are shown in Fig. 7(a). It is clearly seen from Fig. 7(a) that the MgO NPs/FLC composites respond faster than pure W301 and the response time shows a strong dependence on MgO NPs concentration. Upon systematic assessment of the response time of the composites with different concentrations of MgO NPs, 0.5 wt% showed the fastest response, which was $\sim 50\%$ faster than the pure FLC. From Fig. 7(a), it is seen that the value of the response time of

pure W301 is 1.6 ms at an applied voltage of 4 V whereas 0.5 wt % MgO NPs doped W301 showed an electro-optic response in 0.8 ms. There is not much difference in the electrical conductivity of the FLC material W301 even after doping with MgO NPs, because some ionic impurities still remain in the host material. A figure showing the change of electrical conductivity of pure and MgO NPs doped W301 samples with frequency is shown in the ESI.† In the study of the effect of MWCNTs on response time of DHFLC,²³ the authors observed a decrease of the response time of the composite due to the decreased rotational viscosity of the DHFLC upon doping with MWCNTs and increased surface anchoring energy of the composite system. The rotational viscosity of the LC material is directly related to its response time as follows:

$$\tau = \frac{\gamma}{P_s E} \quad (2)$$

where τ is the response time, γ is the rotational viscosity, P_s is the spontaneous polarization, and E is the applied electric field. It is seen from Fig. 7(b) that the rotational viscosity of the FLC material W301 is decreased upon doping with MgO NPs, which is in good agreement with the above mentioned relationship. At 0.5 wt% doping concentration of MgO NPs, the rotational viscosity of the composite became almost half the saturation value of the pure FLC material, and because of this the fastest response is observed there. The reduction in rotational viscosity is attributed mainly to two reasons. First, due to the non-trivial dielectric anisotropic properties of the MgO NPs and FLC material, both experience a torque upon the application of the electric field and hence rotational viscosity is decreased. Second, perturbations in order parameters such as spontaneous polarization and optical tilt angle of the FLC material upon doping with MgO NPs reduce the rotational viscosity of the FLC. Fig. 7(c) and (d) show the variation of the spontaneous polarization and optical tilt angle with applied voltage of pure FLC W301 and MgO NPs doped samples. A clear perturbation in the values of the spontaneous polarization and optical tilt is seen from the figures (Fig. 7(c) and (d)), where at the optimum concentration of MgO NPs (0.5 wt%) dopant, the value of the

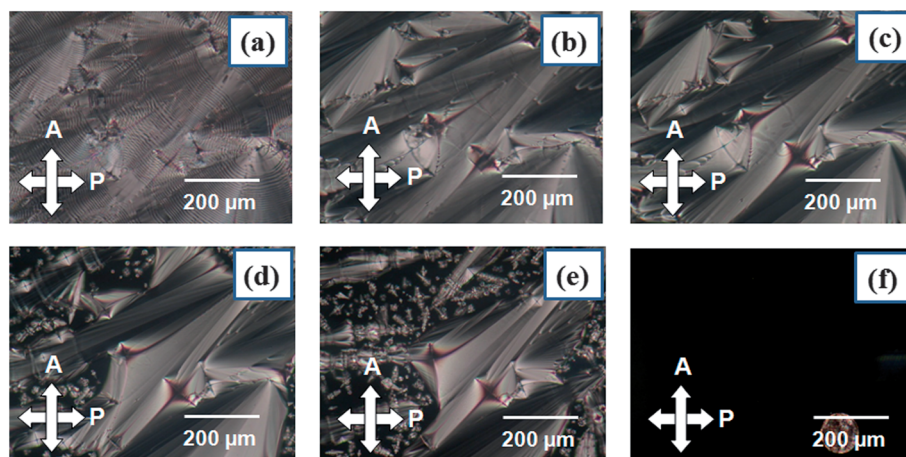


Fig. 6 Optical micrographs of the FLC material W301 at (a) 30°C , (b) 59°C , (c) 70°C , (d) 80.5°C , (e) 80.7°C , and (f) 80.8°C .

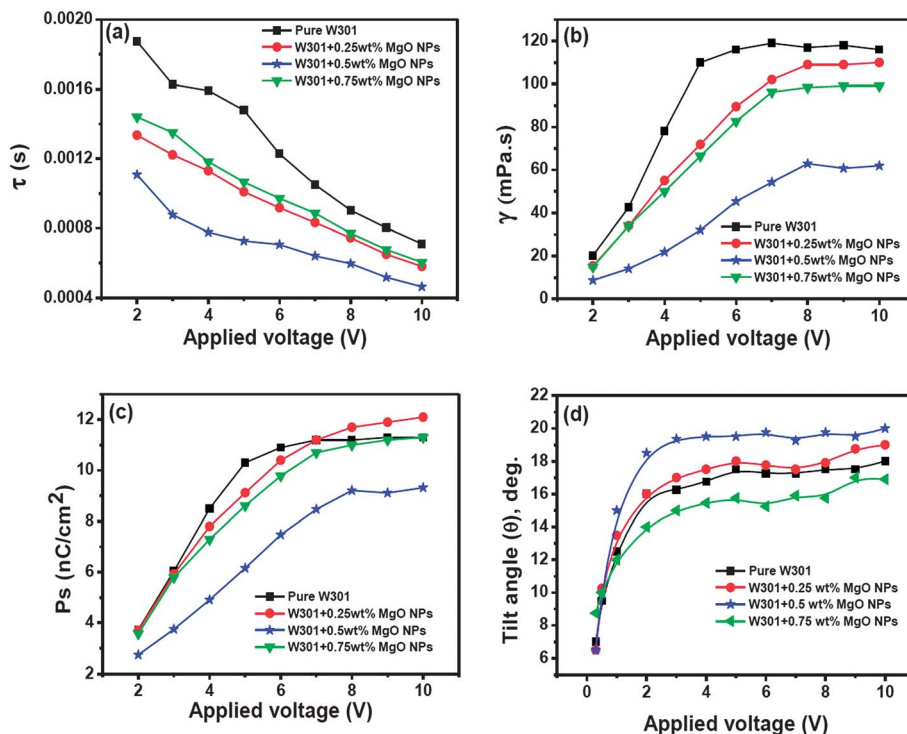


Fig. 7 Behaviour of (a) response time (τ), (b) rotational viscosity (γ), (c) spontaneous polarization (P_s), and (d) optical tilt angle (θ) of pure FLC material W301 and that doped with different concentrations of MgO NPs at room temperature.

spontaneous polarization is decreased and the optical tilt is increased.

Surface anchoring energy and cell gap of the LC also play a key role in the LC response time.³³ The relationship between the response time and anchoring energy for strong anchoring is as follows:

$$\tau = \frac{\gamma}{K_{33}\pi^2} \left(d^2 + \frac{4dK_{33}}{W} \right) \quad (3)$$

where τ is the response time, γ is the rotational viscosity, K_{33} is the bent elastic constant, d is the cell gap and W is the anchoring energy strength coefficient. It is clear from the above mentioned equation that the response time is reduced upon increasing the anchoring energy strength. The elastic energies of the mesogens are increased upon doping with NPs due to the strong anchoring between the LC and the NPs, and therefore attributed to increase in elastic constant.³⁴ The surface defects on the MgO NPs are responsible for this increase in anchoring energy. To confirm the presence of surface defects on the MgO NPs, photoluminescence (PL) characterization was performed. The PL emission spectrum at an excitation wavelength of 250 nm is shown in Fig. 8.

Fig. 8 shows the plot of the PL intensity with wavelength for as-synthesized magnesium hydroxide ($\text{Mg}(\text{OH})_2$) NPs and MgO NPs which are annealed at 300 °C, 500 °C, and 800 °C. MgO generally does not show PL due to its wide-band gap. However, Xie *et al.*³⁵ have reported the occurrence of luminescence in MgO owing to the charge transfer in the surface state. The PL emission in the MgO NPs is attributed to the presence of surface

defects/oxygen vacancies on its surface.³⁶ An incomplete oxidation process during the transformation of $\text{Mg}(\text{OH})_2$ into MgO NPs is responsible for oxygen vacancies on the surface, which may give PL emission.^{36–39} The broad and asymmetric emission peak which is centred in the blue region of the spectrum with high intensity in the PL spectra of MgO NPs is assigned to the structural defects during synthesis.⁴⁰ Thus, the PL study confirms the presence of surface defects on the MgO NPs due to oxygen vacancies. Here, from the PL characteristics of the MgO NPs (Fig. 8), it is clear that the most surface defects due to anion vacancies occur for the MgO NPs which are

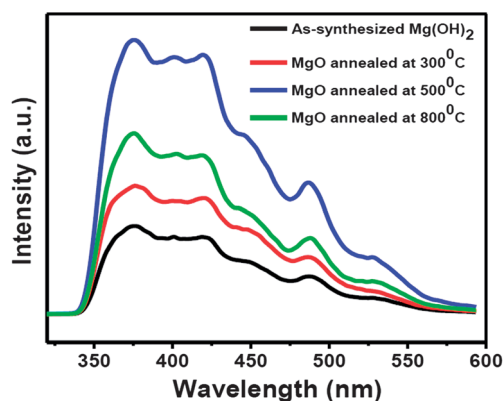


Fig. 8 A comparison of PL emission spectra (excited at 250 nm) of as synthesized $\text{Mg}(\text{OH})_2$ and MgO NPs at different annealing temperatures.

annealed at 500 °C. So, we chose these NPs of MgO, which have higher numbers of surface defects, for making the MgO NPs/FLC composites in our study. Also, researchers have shown theoretically that, for having high chemical activity, oxygen vacancies are essential in the surfaces of MgO NPs.^{18,41} It is seen that MgO NPs with polyhedral or hexagonal shapes possess more defects than typical cubic shaped particles.⁴² In our case, the particles are rounded-polyhedra (Fig. 1(a)), which is an indication of more surface defects. Thus, due to the reduction in viscosity and increase in surface anchoring strength upon the doping of MgO NPs, the composite shows a faster response.

Enhancement in optical tilt angle and contrast of MgO NPs/FLC composites

As seen in Fig. 7(d), the optical tilt angle is enhanced upon doping with MgO NPs and has a strong dependence on the MgO NPs concentration. From Fig. 7(d), it is clear that the value of the optical tilt angle is the highest for 0.5 wt% MgO NPs/FLC composites. The same concentration of MgO NPs showed the fastest response. Therefore, this is the optimum concentration for a faster response with an improved tilt angle for the composites. Here, upon doping with 0.5 wt% of MgO NPs the value of the tilt angle showed an increase of $\sim 2.5^\circ$ for all applied voltages above 1 V. An enhancement in the optical tilt angle of the FLC is reported in ref. 43 and 44, where the authors doped the FLC with selenium docosane capped palladium NPs and gold nanoparticles, respectively, and the steric interaction between the NPs and mesogens improved the tilt in the former case and resulted in the generation of a strong intrinsic field in the latter. It is reported that the (111) plane of MgO, which contains either a layer of magnesium cations or a layer of oxygen anions, is not charge neutral.¹⁶ The MgO NPs used in this study have a non-zero dipole moment along the (111) plane (ref.: JCPDS file no. 870652, lattice parameter: $a = 0.4211$ nm). Thus the MgO NPs having an inherent dipole moment interact with the dipolar mesogens, which results in the improvement of the optical tilt angle. In addition to this, the MgO NPs used in this study have high numbers of surface defects, which arises due to the oxygen vacancies on the surface. Upon the application of the electric field, these defective surface sites interact electrostatically with dipolar mesogens and offer strong surface anchoring. Improvement in the optical tilt ultimately leads to the improvement of contrast of LC displays.

Fig. 9 shows a schematic diagram of the interaction of MgO NPs with mesogens. Due to the dipole-dipole interaction between the FLC molecules and NPs a strong intrinsic field inside the sample is created. Previously, some studies have reported that the enhancement of the local electric field due to the doping of NPs can be attributed to faster response characteristics.^{21,45}

The loosening of the helical packing of molecules, which reduces the rotational viscosity and the anchoring of mesogens on the surface of MgO, is displayed in this schematic (Fig. 9).

The optical micrographs indicating the dark and bright states of pure (Fig. 10(a) and (b)) and doped samples (Fig. 10(c) and (d))

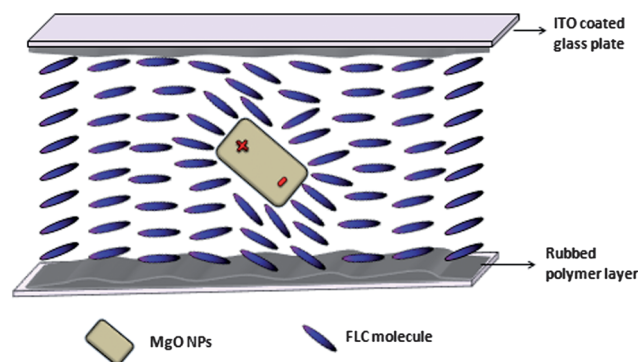


Fig. 9 Schematic representation of MgO NPs doped W301 material filled cell.

and (d)) are shown. From this figure it is seen that the molecular alignment of the FLC material W301 is improved upon doping with MgO NPs. The light leakage in the dark state of the doped samples (Fig. 10(c)) is also reduced, giving an improved darkness due to the dipole-dipole interaction and increase of surface anchoring strength of the FLC with NPs. The bright state (Fig. 10(d)) also shows an improved texture compared to pure W301 (Fig. 10(b)).

For quantifying this, we considered the variation of the optical spectrum intensity with wavelength for pure and doped samples. Fig. 11 shows the fitted data of the optical spectrum intensity *versus* wavelength from the spectrum analyser for the pure and doped samples in the dark state (Fig. 11(a)) and bright state (Fig. 11(b)).

It is clearly seen from the Fig. 11(a) that the intensity of the dark state is less for the doped sample while the intensity of bright state is almost doubled (Fig. 11(b)) compared to the pure W301. A clear confirmation of the improvement of the contrast is obtained from this: the dark state of the sample became darker and the bright state became brighter upon doping with MgO NPs.

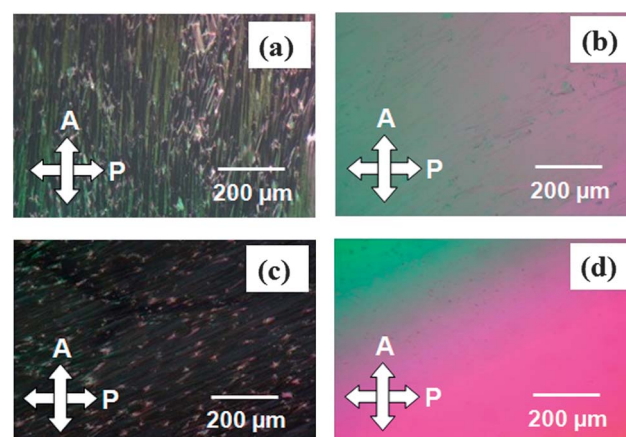


Fig. 10 Polarizing optical micrographs showing (a) dark and (b) bright states of pure W301 material and (c) dark and (d) bright states of MgO NPs doped W301 material filled sample cells of thickness 6 μm at room temperature. Scale bar: 200 μm . Crossed arrows represent crossed polarizer (P) and analyzer (A).

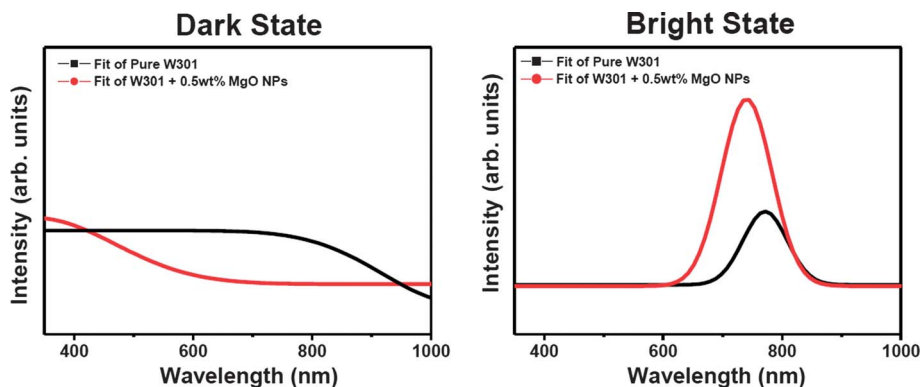


Fig. 11 The fitted data for the optical spectrum intensity versus wavelength from the spectrum analyser for the pure W301 and MgO NPs doped sample in the (a) dark state and (b) bright state.

Conclusions

We have presented the preparation and characterization of a new FLC material, W301, and the concentration dependent doping effects of the MgO NPs on the host FLC for the improvement of the response time and contrast of MgO NPs/FLC composites. The role of rotational viscosity and surface anchoring strength on the increased speed of response is systematically discussed. Additionally, the enhancement of the tilt angle and contrast is discussed, which is attributed to the dipole-dipole interaction of mesogens and NPs along with the improvement in the surface anchoring strength. These studies would be helpful for the development of future fast responding LC display devices having improved contrast.

Acknowledgements

The authors sincerely thank Professor R. C. Budhani, Director, CSIR-National Physical Laboratory, New Delhi for continuous encouragement and interest in this work. We sincerely thank Mr Tilak Joshi, Mr S. Tripathi, Dr A. Malik, Dr A. Kumar and Dr A. Choudhary for useful discussions. We also thank Dr D. Haranath for fruitful discussions. The author A. C. thanks the Council of Scientific and Industrial Research (CSIR) for providing financial assistance, and the author J. P. is grateful to the Department of Science and Technology for supporting this work under the INSPIRE Faculty Award (DST/INSPIRE Faculty Award/2011) through the INSPIRE Faculty Scheme of DST [IFA-PH-10].

References

- 1 J. W. Goodby, *Liq. Cryst.*, 2011, **38**, 1363.
- 2 S. Gauza, X. Zhu, W. Piecek, R. Dąbrowski and S.-T. Wu, *J. Disp. Technol.*, 2007, **3**, 250.
- 3 J. W. Goodby, R. Blinc, N. A. Clark, S. T. Lagerwall, M. A. Osipov, S. A. Pikin, T. Sakurai, K. Yoshino and B. Zeks, *Ferroelectric Liquid Crystals*, Gordon and Breach, Amsterdam, 1991, part II, p. 410.
- 4 K. Yoshino, K. G. Balakrishnan, T. Uemoto, Y. Iwasaki and Y. Inuishi, *Jpn. J. Appl. Phys.*, 1978, **17**, 597.
- 5 G. Andersson, I. Dahl, W. Kuczynski, S. T. Lagerwall, K. Skarp and B. Stebler, *Ferroelectrics*, 1988, **84**, 285.
- 6 S. Kaur, A. K. Thakur, S. S. Bawa and A. M. Biradar, *Appl. Phys. Lett.*, 2006, **88**, 122905.
- 7 M. Suzuki, H. Furue and S. Kobayashi, *Mol. Cryst. Liq. Cryst.*, 2001, **368**, 191.
- 8 Y. H. Chen and W. Lee, *Appl. Phys. Lett.*, 2006, **88**, 222105.
- 9 S. P. Chen, C. C. Huang, W. Y. Liu and Y. C. Chao, *Appl. Phys. Lett.*, 2007, **90**, 211111.
- 10 Y. Shiraishi, N. Toshima, K. Maeda, H. Yoshikawa, J. Xu and S. Kobayashi, *Appl. Phys. Lett.*, 2002, **81**, 2845.
- 11 Y. Du and N. Toshima, *Bull. Chem. Soc. Jpn.*, 2007, **80**, 2446.
- 12 *Synthesis, Properties and Applications of Oxide Nanoparticles*, ed. J. A. Rodríguez and M. Fernández-García, Wiley, New Jersey, 2007.
- 13 M. Valden, X. Lai and D. W. Goodman, *Science*, 1998, **281**, 1647.
- 14 J. A. Rodríguez, G. Liu, T. Jirsak, J. Hrbek, Z. Chang, J. Dvorak and A. Maiti, *J. Am. Chem. Soc.*, 2002, **124**, 5247.
- 15 M. L. Trudeau and J. Y. Ying, *Nanostruct. Mater.*, 1996, **7**, 245.
- 16 A. M. Föller, *Magnesium Oxide and its Applications*, Vollhardt, Berlin, 1978.
- 17 Z. Dohnálek, G. A. Kimmel, D. E. McCready, J. S. Young, A. Dohnáková, R. S. Smith and B. D. Kay, *J. Phys. Chem. B*, 2002, **106**, 3526.
- 18 G. Pacchioni and P. Pescarmona, *Surf. Sci.*, 1998, **412/413**, 657.
- 19 Y. Shiraishi, K. Sugihara, N. Okamura, H. Sawai, S. Kobayashi and N. Toshima, *Macromol. Symp.*, 2012, **317-318**, 28-33.
- 20 D. J. Gardiner, S. M. Morris, F. Castles, M. M. Qasim, W. S. Kim, S. S. Choi, H. J. Park, I. J. Chung and H. J. Coles, *Appl. Phys. Lett.*, 2011, **98**, 263508.
- 21 A. Mikulko, P. Arora, A. Glushchenko, A. Lapanik and W. Haase, *Europhys. Lett.*, 2009, **87**, 27009.
- 22 S. Ghosh, P. Nayek, S. K. Roy, R. Gangopadhyay, M. R. Molla and T. P. Majumder, *Eur. Phys. J. E: Soft Matter Biol. Phys.*, 2011, **34**, 35.
- 23 J. Prakash, A. Choudhary, D. S. Mehta and A. M. Biradar, *Phys. Rev. E: Stat., Nonlinear, Soft Matter Phys.*, 2009, **80**, 012701.

- 24 A. Malik, J. Prakash, A. Kumar, A. Dhar and A. M. Biradar, *J. Appl. Phys.*, 2012, **112**, 054309.
- 25 F. Haraguchi, K. Inoue, N. Tushima, S. Kobayashi and K. Takatoh, *Jpn. J. Appl. Phys.*, 2007, **34**, L796.
- 26 S. Sano, T. Miyama, K. Takatoh and S. Kobayashi, *Proc. SPIE 6135, Liquid Crystal Materials, Devices, and Applications XI*, 23 February 2006, p. 613501.
- 27 H. Zschke, *J. Prakt. Chem.*, 1975, **317**, 617.
- 28 P. Kula, K. Herman and O. Chojnowska, *Liq. Cryst.*, 2013, **40**, 83.
- 29 A. M. Biradar, S. Wróbel and W. Haase, *Phys. Rev. A*, 1989, **39**, 2693.
- 30 A. Levstik, T. Carlsson, C. Filipic, I. Levstik and B. Zeks, *Phys. Rev. A: At., Mol., Opt. Phys.*, 1987, **35**, 3527.
- 31 S. Hiller, L. A. Beresnev, S. A. Pikin and W. Haase, *Ferroelectrics*, 1996, **180**, 153.
- 32 S. Worbelt, A. M. Biradar and W. Haase, *Ferroelectrics*, 1989, **100**, 271.
- 33 X. Nie, R. Lu, H. Xianyu, T. X. Wu and S. T. Wu, *J. Appl. Phys.*, 2007, **101**, 103110.
- 34 S. Y. Jeon, S. H. Shin, S. J. Jeong, S. H. Lee, S. H. Jeong, Y. H. Lee, H. C. Choi and K. J. Kim, *Appl. Phys. Lett.*, 2007, **90**, 121901.
- 35 S. Xie, X. Han, Q. Kuang, Y. Zhao, Z. Xie and L. Zheng, *J. Mater. Chem.*, 2011, **21**, 7263.
- 36 B. M. Maoz, E. Tirosh, M. B. Sadan, I. Popov, Y. Rosenberg and G. Markovich, *J. Mater. Chem.*, 2011, **21**, 9532.
- 37 L. Kumari, W. Z. Li, C.-H. Vannoy, R.-M. Leblanc and D.-Z. Wang, *Ceram. Interfaces*, 2009, **35**, 3355.
- 38 K. Krishnamoorthy, J. Y. Moon, H. B. Hyun, S. K. Cho and S. J. Kim, *J. Mater. Chem.*, 2012, **22**, 24610.
- 39 Y. Hao, G. Meng, C. Ye, X. Zhang and L. Zhang, *J. Phys. Chem. B*, 2005, **109**, 11204.
- 40 H. B. Lu, L. Liao, H. Li, Y. Tian, J. C. Li, D. F. Wang and B. P. Zhu, *J. Phys. Chem. C*, 2007, **111**, 10273–10277.
- 41 A. M. Ferrari and G. Pacchioni, *J. Phys. Chem.*, 1996, **100**, 9032.
- 42 K. J. Klabunde, J. Stark, O. Koper, C. Mobs, D. G. Park, S. Decker, Y. Jiang, I. Lagadic and D. Zhang, *J. Phys. Chem.*, 1996, **100**, 12142.
- 43 A. Kumar, G. Singh, T. Joshi, G. K. Rao, A. K. Singh and A. M. Biradar, *Appl. Phys. Lett.*, 2012, **100**, 054102.
- 44 S. Kaur, S. P. Singh, A. M. Biradar, A. Choudhary and K. Sreenivas, *Appl. Phys. Lett.*, 2007, **91**, 023120.
- 45 A. Lapanik, A. Rudzki, B. Kinkead, H. Qi, T. Hegmann and W. Haase, *Soft Matter*, 2012, **8**, 8722.